

Self-assembly of 3D Carbon Nanotube Sponges: A Simple and Controllable Way to Build Macroscopic and Ultralight Porous Architectures

Shu Luo, Yufeng Luo, Hengcai Wu, Mengya Li, Lingjia Yan, Kaili Jiang,* Liang Liu, Qunqing Li, Shoushan Fan, and Jiaping Wang*

Carbon nanotube (CNT) is one of the most intensively explored carbon materials due to its unique properties with high electrical conductivity (10^5 S cm^{-1}),^[1] large thermal conductivity ($6000 \text{ W m}^{-1} \text{ K}$), and superior mechanical properties.^[2] In order to use this fabulous nanomaterial in practical applications, microsized (or nanosized) CNTs are usually required to be assembled into macroscopic architectures. Building CNTs into long fibers or 2D films has gained great achievements in the fields of energy storage, catalysis, electronics, bioengineering, etc.^[3–13] However, in a broader range of fields, 3D CNT architectures with specific shapes and volumes are usually needed to satisfy the spatial requirements and to increase the amount of active material.^[14] CNT sponge, as a typical representative 3D CNT architecture, has attracted more and more attention among researchers in recent years.^[14–21] As a classic macroscopic construction, CNT sponge exhibits unique porous and hierarchical structure, consisting of macro-, meso-, and micropores. The macropores and open structure in the sponge are beneficial for the mass transfer, while the meso- and micropores can provide high surface areas and abundant reactive points.^[14]

To obtain CNT sponges, many efforts have been made. However, up till now, the methods for fabricating CNT-based sponges are quite limited. The most-widely explored way was to obtain aqueous suspensions of CNTs with the aid of organogelators such as surfactants, polyvinyl alcohol (PVA), or other polymers, and then obtain freestanding CNT aerogels by freeze or supercritical CO_2 drying processes.^[14,17,22–26] In this structure, CNTs were glued by the organic binder, which inevitably decreased the surface activity of CNTs and reduced the conductivity and chemical stability of the sponges.^[14,22,24] Although the organic binders can be turned into amorphous carbon through

pyrolysis, the amount of carbon was too much and not easy to control.^[22,27] To obtain pure CNT sponges, Wu and co-workers used a chemical vapor deposition (CVD) method and obtained pure interconnected CNT sponges, which possessed great conductive and mechanical properties.^[15,16] However, from a practical point of view, more efforts need to be done in finding an easy-to-control and scalable method with great potential for massive production of pure CNT sponges.

Here, we report the construction of pure CNT sponges with superaligned CNTs (SACNTs) through a simple self-assembly method (Figure 1a). Different from ordinary CNTs, SACNT arrays are well-aligned, compact, and have very clean surfaces. Generally, clean surfaces lead to strong van der Waals interaction. SACNT arrays can be converted into continuous yarns or films by an end-to-end joining mechanism, originating from the strong van der Waals interactions between neighboring CNTs in the superaligned arrays.^[4,28] In 2012, we reported an ultrasonication and codeposition method to fabricate SACNT/LiCoO₂ (or other materials in powder forms) composites, and found that SACNTs were able to form a continuous and monolithic 3D network in solvent after ultrasonication. Such method and phenomenon did not apply for ordinary CNTs, demonstrating the important role of the strong interaction in SACNTs in forming a continuous 3D network.^[29] With this unique property of SACNTs, microsized SACNTs can easily self-assemble into macroscopic 3D sponges via a simple ultrasonication and freeze-drying procedure, without using any organic binder or templates as most solution-based methods do. In this pure SACNT sponge, SACNTs are integrated through the strong van der Waals force, thus the intrinsic properties of SACNTs can be preserved.

By changing the shapes of the containers and the concentration of SACNTs in suspensions, macroscopic SACNT sponges with specific shapes and controllable densities can be easily achieved, from as low as 1 mg cm^{-3} to more than 50 mg cm^{-3} in a continuous range. These SACNT sponges are in a honeycomb-like hierarchical 3D structure, combining micro-, meso-, and macropores together, in which the pore-size distribution is determined by the density of the sponge. These SACNT sponges share the advantages of extremely low density ($\approx 1 \text{ mg cm}^{-3}$), high porosity >99%, wettability to organics, and highly conductive network. Moreover, the simplicity and full controllability of the assembly process also provide the SACNT sponges with great potential in massive and low-cost manufacture. Meanwhile, as there is no need for binders in forming pure SACNT sponges, improved chemical/thermal stability

Dr. S. Luo, Y. F. Luo, Prof. S. S. Fan
Department of Physics and Tsinghua-Foxconn
Nanotechnology Research Center
School of Materials Science and Engineering
Tsinghua University
Beijing 100084, China

H. C. Wu, M. Y. Li, L. J. Yan, Prof. K. L. Jiang,
Dr. L. Liu, Prof. Q. Q. Li, Prof. J. P. Wang
Department of Physics and Tsinghua-Foxconn
Nanotechnology Research Center
Tsinghua University
Beijing 100084, China
E-mail: jiangkl@tsinghua.edu.cn; jpwang@tsinghua.edu.cn



DOI: 10.1002/adma.201603549

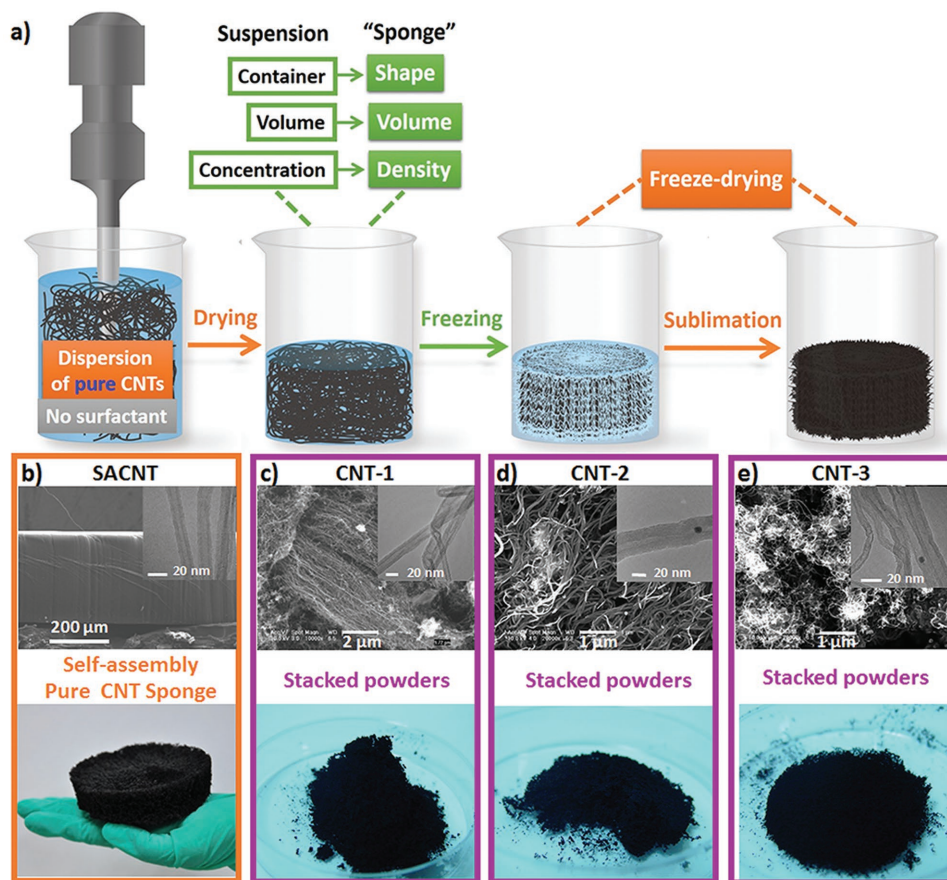


Figure 1. a) Schematic of the fabrication process for CNT sponges. Microstructures of CNTs and the obtained products for b) SACNT, c) CNT-1, d) CNT-2, and e) CNT-3.

and surface reactivity can be achieved, leading to broader and extended fields of applications, such as electronics, energy storage, bioengineering, catalysis, environmental treatment, and so on.

Figure 1a shows the fabrication process of pure CNT sponges through an ultrasonication and freeze-drying procedure without using any organic binder. As shown in Figure 1b–e and Figure S1a (Supporting Information), five kinds of CNTs were used: SACNT arrays with two different heights, ordinary CNT arrays (CNT-1), relatively straight CNTs (CNT-2), and twisted CNTs (CNT-3), in which CNT-1, CNT-2, and CNT-3 were in powder form. The heights of SACNT arrays were 300 μm and 10–20 μm , respectively, and the diameter of a single SACNT was about 10 nm. For CNT-1, 2, 3, the lengths of CNTs were all around 10 μm , while the diameters were 10, 20, and 10 nm, respectively. Among these five kinds of CNTs, both long and short SACNTs arrays can self-assemble into freestanding and macroscopic sponges by the ultrasonication and freeze-drying procedure (Figure 1b and Figure S1, Supporting Information). While for the other three kinds of CNTs, the obtained products were loosely stacked clusters, which would easily break into separated powders (Figure 1c–e).

As demonstrated in previous papers, the conversion of SACNT arrays into continuous CNT film originates from the strong van der Waals interaction between neighboring

CNTs.^[4,28] Similarly, the ability in forming CNT sponges is also determined by the interaction among CNTs. For both long and short SACNTs, they have high purity and clean surfaces (Figure S2, Supporting Information), so that the neighboring CNTs kept close together and the van der Waals interaction among CNTs was strong enough to form a continuous network and then self-assemble into a freestanding sponge. Therefore, the capability of forming sponges is not affected by the length of SACNTs. Instead, the strong van der Waals interaction among CNTs plays the key role. In comparison, the other three kinds of CNTs were not able to form sponges. In these ordinary CNTs, there existed large amount of amorphous carbon and impurities such as catalyst particles on the tube sidewalls with rough surfaces (Figure S2, Supporting Information), which increased the distance among the tubes and resulted in weak van der Waals interaction among CNTs. The dispersive states of CNTs after ultrasonication were further studied. As shown in Figure 2a, SACNTs immediately self-assembled into an integrated cloud after the ultrasonication process and no fragments were found in the surrounding solution. A droplet from the SACNT suspension was placed onto an Al foil and observed under an optical microscope (left) and a scanning electron microscope (SEM, right). SACNTs on the Al foil connected together and formed a continuous network. These results demonstrated that SACNTs were overall connected and

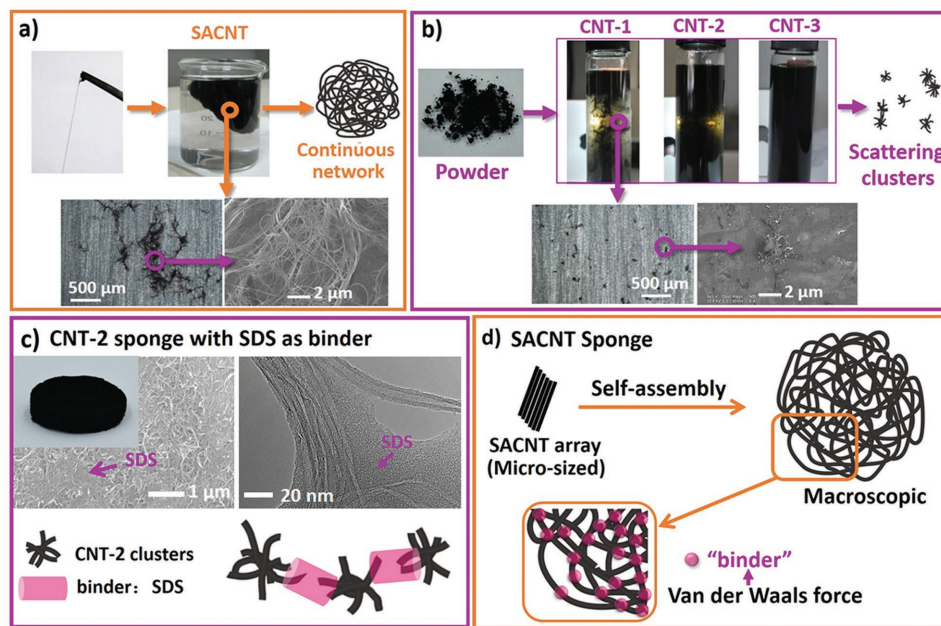


Figure 2. Dispersion state of a) SACNTs and b) ordinary CNTs after ultrasonication. c) Microstructure (left: SEM image, right: TEM image), photograph, and the assembly model of CNT-2 sponge with SDS as binder. d) The assembly model of SACNT sponge, where the van der Waals force among SACNTs serves as a “binder” to “glue” all the SACNTs together into a macroscopic network.

self-assembled into a continuous and macroscopic 3D network. Although the external force from ultrasonication tended to break SACNTs apart and make them randomly separated, the strong van der Waals interaction kept the neighboring SACNTs well connected. Therefore, SACNTs joined with one another and integrated into a continuous network.

On the contrary, ordinary CNTs in the powder form were dispersed uniformly in the solvent, and the suspensions were totally black after ultrasonication (Figure 2b). With the aid of flashlight behind the suspensions, it can be found that hundreds of small and separated clusters were suspended in the solvent. One droplet of such suspension was placed onto an Al foil, displaying small and totally separated clusters composed of many isolated groups of CNTs. These CNT clusters were not able to assemble together due to the surface defects and weak interaction among ordinary CNTs.

To obtain a sponge with ordinary CNTs, adequate surfactants such as sodium dodecyl sulfonate (SDS) were added into the CNT suspensions (weight ratio of CNT-2:SDS at 1:5), dispersed by ultrasonication, rested for 24 h, and then underwent freeze-drying to form an aerogel. A freestanding sponge with CNT-2 and SDS is shown in Figure 2c, and according to the SEM and transmission electron microscope (TEM) images, CNTs were covered and connected by SDS, demonstrating the role of SDS as a binder to glue CNTs together. In contrast, SACNTs were capable of self-assembling into a continuous network and forming pure SACNT sponges without binder. As discussed above, the strong Van der Waals force is the key point that integrates all the SACNTs together. Therefore, the role of strong Van der Waals force among SACNTs can be identified as the “binder” to “glue” all SACNTs together (Figure 2d), similar to the function of SDS in the CNT-2 sponge. The van der Waals force as “binder” does not affect the intrinsic properties of

SACNTs in the sponges, while organic binders such as SDS may greatly decrease the surface activity of CNTs and affect both thermal/chemical stability and electrical conductivity of ordinary CNT aerogels.

Because of the simplicity and full controllability of the self-assembly process in the binder-free and template-free methodology, macroscopic and pure SACNT sponges with specific shapes, sizes, and controllable densities were achieved by changing the shapes of the containers and the concentration of SACNTs in suspensions. Moreover, these sponges can be readily cut into smaller objects with designed shapes and even finer structures through laser cutting. SACNT sponges with desired shapes and sizes, such as letters spelling “TFNRC,” animal form (rabbit and fish), smiling face, rods, disks, and cylinders are shown in Figure 3a. On the contrary, it was difficult to slice ordinary CNT sponges with organic binders into desired shapes through laser cutting due to the poor thermal conductivity and probable fusion of the organic binder. SACNT sponges can also be easily manufactured in a large-scale way. For example, an SACNT sponge disk with diameter of 20 cm and volume of nearly 1000 cm³ was made with a mold of 1 L plate. Actually, the dimensions of the SACNT sponges could be much larger as long as the cavity of the freeze-drying or supercritical extraction equipment is big enough.

SACNT sponges with different densities and porosities were achieved in a completely controllable way, from as low as 1 mg cm⁻³ to more than 50 mg cm⁻³ as needed. Despite their various densities, these sponges were all highly porous and extremely light weight. The relatively compact sponges with a density of 50 mg cm⁻³ possessed a porosity of about 97.5%–98%. While for the lightest sponges (1 mg cm⁻³), the porosity was over 99.9%. This SACNT sponge is the lightest among pure CNT sponges reported so far, and is also one of the

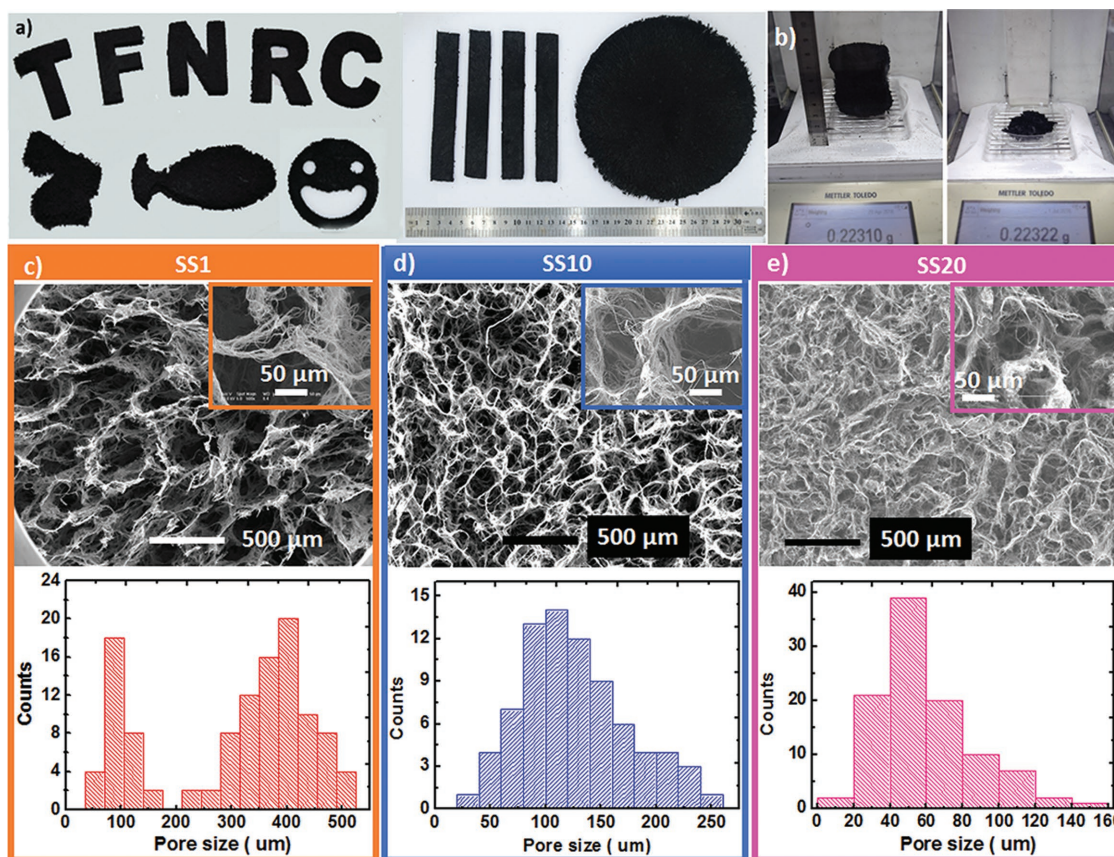


Figure 3. a) Photographs of SACNT sponges with diverse shapes and sizes. b) Photographs of ≈ 220 mg SACNT sponge (density: 2 mg cm^{-3}) and SACNT arrays. SEM images and pore size distributions of SACNT sponges with different densities: c) 1 mg cm^{-3} (SS1), d) 10 mg cm^{-3} (SS10), and e) 20 mg cm^{-3} (SS20).

lightest among pure carbon sponges.^[15–17,19,20,30] As shown in Figure 3b, about 220 mg of the ultralight SACNT sponge (2 mg cm^{-3}) and SACNT arrays were weighed, respectively. SACNTs in the array form were tightly contacted and occupied a small volume. After the ultrasonication and freeze-drying procedure, SACNTs self-assembled into a 3D macroscopic and highly porous sponge that occupied a volume about 100 times larger than the arrays.

Figure 3c–e and Figure S3 (Supporting Information) display the SEM images of SACNT sponges with different densities at 1 mg cm^{-3} (SS1), 10 mg cm^{-3} (SS10), 20 mg cm^{-3} (SS20), and 40 mg cm^{-3} (SS40), respectively. All of these SACNT sponges presented a honeycomb-like 3D structure, in which the cell walls of the “honeycomb” were composed of SACNT bundles. The construction of this honeycomb-like structure is template-free, implying the spontaneous formation of this unique structure due to the interaction between the dispersing medium (water in this work) and SACNTs during the self-assembly process. The cell size distribution of the honeycomb, which was also the pore size of the sponge, varied with the density of the sponges, usually ranging from hundreds of micrometers to tens of micrometers. For SS1, the cell diameters were divided into two ranges, mainly distributed among 300–500 μm and 50–150 μm , which were typical macropores. While on the cell walls, as shown in the inset image in Figure 3c, the pores among the SACNT

bundles were in the range of several nanometers to tens of micrometers, which possessed both meso- and macropores. Considering the micropores within the SACNT inner tubes, these SACNT sponges exhibited a hierarchical structure combining macro-, meso-, and micropores together. SS10, SS20, and SS40 exhibited similar hierarchical porous structures, and the only differences lied in the cell size and the porosity of the cell walls. The cell size distributions were mainly among 50–225 μm in SS10, 20–80 μm in SS20, and 20–60 μm in SS40. For the cell walls, they became more compact and less porous when the density of the sponges increased.

In this hierarchical honeycomb-like structure, macropores in the sponges were connected and formed an interconnected assembly of open inner channels throughout the sponges. Therefore, it is favorable for mass transport and accessibility to the inner surface all over the sponges. In addition, the meso- and micropores in the sponges can lead to high surface area, which provides plenty of positions for absorption or adhesion, and reactive points to increase the reaction activity and efficiency of the sponges.

The electrical conductivities of the SACNT sponges with different densities were characterized. The current–voltage curves for pure SACNT sponges in Figure 4a exhibited perfect linear correlation, indicating an ohmic behavior. The electrical conductivities of the SACNT sponges (SS1, SS10, and SS20) were

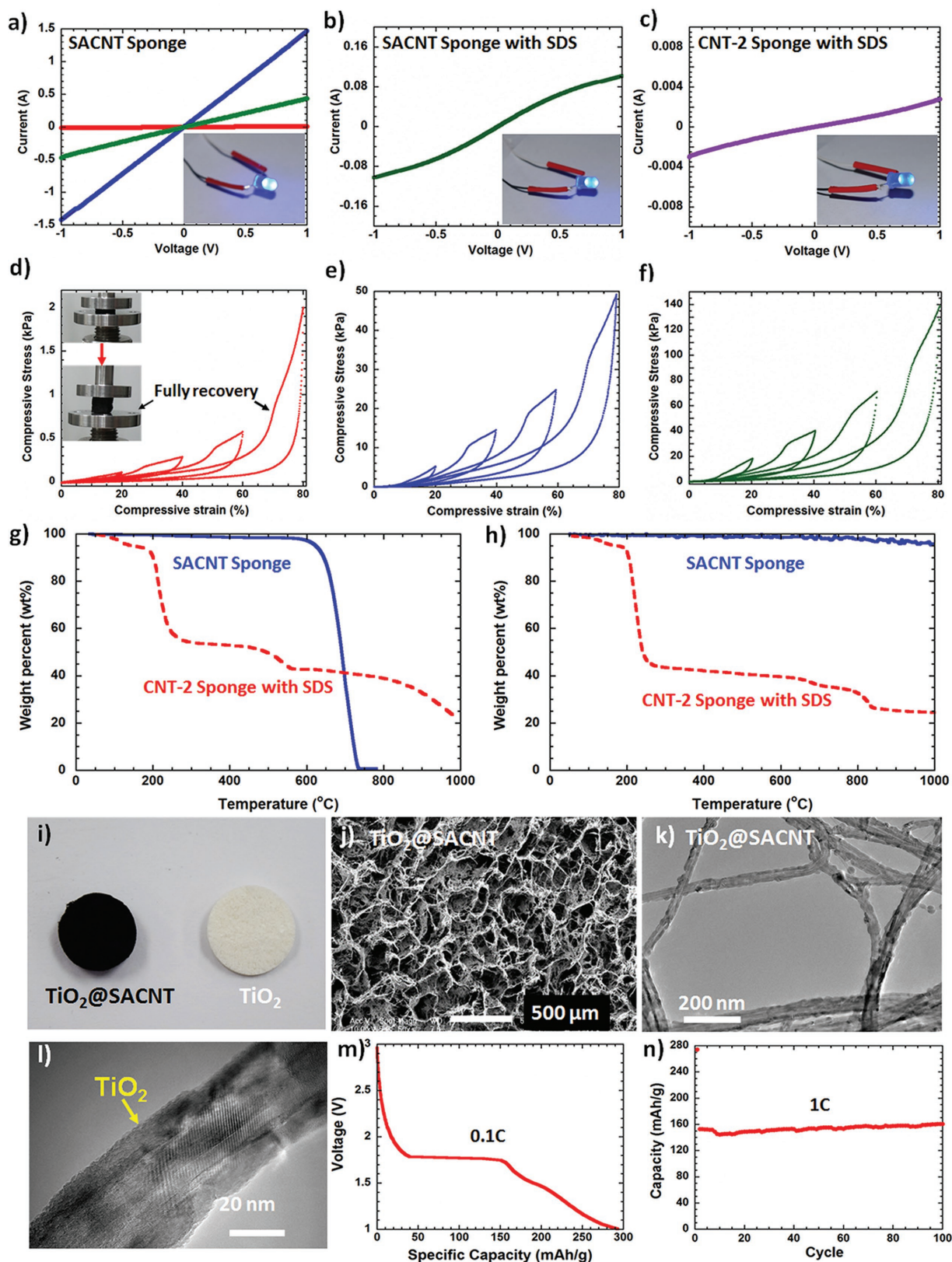


Figure 4. Current–voltage curves of a) SACNT sponge, b) SACNT sponge with SDS, c) CNT-2 sponge with SDS; Compressive stress–strain curves of d) SS1, e) SS10, and f) SS20 sponges with carbon coating; Compressive TGA results of SACNT sponge and CNT-2 sponge with SDS in g) air and h) Ar atmosphere. i) Photograph, j,k,l) SEM and TEM images, and m,n) electrochemical properties of TiO₂@SACNT composite.

calculated to be 0.015, 0.44, and 1.25 S cm⁻¹, respectively. With SDS binder, both SACNT sponges and ordinary CNT sponges were obtained and their electrical conductivities were also tested. As shown in the current–voltage curves in Figure 4b, SACNT sponge (SS10) with SDS displayed a nonlinear current–voltage curve, and the electrical conductivity could be approximated as 0.1 S cm⁻¹, which was about 77% lower than the pure SACNT sponge. As for the CNT-2 sponge with SDS, the electrical conductivity was only 0.003 S cm⁻¹ (Figure 4c), about two orders of magnitude lower than the pure SACNT sponge. Due to the presence of the organic binder, both SACNT-SDS and CNT-2-SDS sponges exhibited lower conductivities than the pure SACNT sponge. The LED lamps connected to the pure SACNT sponge, SACNT sponge with SDS, and CNT-2 sponge with SDS under 3 V showed the highest, medium, and least brightness (inset photos in Figure 4a–c), demonstrating the advantage of the high electrical conductivity for the pure SACNT sponges.

The compressive properties of SACNT sponges were investigated. As shown in Figure S4a (Supporting Information), pure SACNT sponge exhibited poor volume recovery after compression and release, which was not satisfactory. With an applied 50% compressive strain, SS10 sponge can only recover 12% of the original volume after release. SS10 sponge with SDS also demonstrated poor volume recovery after compression and release (Figure S4b, Supporting Information), and showed an increase in the compressive stress at 50% strain compared to SS10. As demonstrated in literature, mechanical properties of CNT sponges can be improved by carbon coating.^[31] With a thin layer of carbon coating (1–2 nm), SACNT sponges became extremely flexible and exhibited full volume and shape recovery under cyclic compression. Figure 4d–f show the compressive stress–strain curves of SS1, SS10, and SS20 sponges with carbon coating, respectively. All of the treated SACNT sponges demonstrated full recovery at high compressive strains even up to 80%. The compressive stresses increased with increasing density of the SACNT sponges, being 2 kPa for SS1, 49 kPa for SS10, and 141 kPa for SS20 at 80% strain. The carbon-coated SACNT sponges can remain stable structure when immersed in solution. After being taken out of the solution and dried, it did not show any apparent deformation or volume reduction (Figure S5, Supporting Information).

Figure 4g demonstrates the results of thermal gravity analysis (TGA) in air for the pure SACNT sponge and the CNT-2 sponge with SDS. The pure SACNT sponge maintained stable structure with no weight loss up to 600 °C. After that, it started to be oxidized by air and completely vanished when the temperature approached 730 °C. This thermal behavior was the same with pure SACNT arrays, therefore the intrinsic thermal property of SACNTs was well preserved in the SACNT sponges. In comparison, the CNT-2 sponge with SDS started to lose weight notably from 200 °C, when SDS began to decompose. The remaining weight after 1000 °C included the oxidized catalysts in CNT-2 and decomposition products of SDS. Figure 4h displays the TGA results of the pure SACNT sponge and the CNT-2 sponge in Ar from 25 °C to 1000 °C. Due to the intrinsic thermal stability of SACNTs in inert gases, the pure SACNT sponge kept stable and showed a weight loss of only 5 wt% up to 1000 °C. Similar to the TGA results in air, the CNT-2 sponge

with SDS in Ar still displayed pyrolysis starting from 200 °C because of the low thermal stability of SDS. TGA results demonstrated that the pure SACNT sponges without binder not only processed the advantage of high electrical conductivity, but also demonstrated high thermal stability.

Due to their unique structure, excellent physical properties, and simplicity in fabrication, these SACNT sponges reveal great potential for various applications, such as absorption, catalysis, energy devices, bioengineering, etc. One of the most promising applications is to use the SACNT sponges as template and prepare honeycomb-like hierarchical materials, such as metals, oxides, and composites. Figure 4i shows a TiO₂@SACNT composite fabricated by coating an SACNT sponge with a 10 nm layer of TiO₂ through atomic layer deposition (ALD) with 56 wt%TiO₂. This composite demonstrated the same honeycomb-like structure with the SACNT sponge (Figure 4j). TEM images exhibited the uniform coating of TiO₂ around the SACNT network (Figure 4k). The TiO₂ coating was mainly crystalline together with some amorphous phase (Figure 4l). In principle, uniform thin film coating can be achieved regardless of the sample size by tuning the ALD process parameters. In this work, the thickness of the TiO₂-coated SACNT sponge was 3 mm, which was limited by the chamber size. Within this dimension range, TEM observation illustrated desired uniformity of TiO₂ coating on the SACNT sponge. Thermal treatment in air (700 °C) for an hour turned this TiO₂@SACNT composite into white TiO₂ sponge, still retaining the honeycomb-like structure (Figure 4i). The TiO₂@SACNT composite can be applied as anode material for lithium ion batteries, and displayed a typical discharge curve of anatase TiO₂, similar to the curves reported in literature.^[32] It showed an initial capacity of 285 mAh g⁻¹ at 0.1 C and stable cycling performance over 100 cycles at 1 C with a capacity of 153 mAh g⁻¹ (Figure 4m,n). These results indicated the effective conducting network, high reactive activity, and excellent stability of the TiO₂@SACNT sponge composite.

Other metal or metal oxide sponges (such as Au, Ag, Cu, Fe₂O₃, SiO₂, and Al₂O₃) in honeycomb-like hierarchical structures could also be achieved through solution method, ALD, or other coating techniques with SACNT sponges as templates. As the honeycomb-like structure of SACNT sponges is completely controllable, the cell size distribution and porosity of the honeycomb structure could be finely adjusted. Therefore, metal or metal oxide sponges with designed hierarchical structures can be achieved. Based on these sponges, studies on the relations between properties and hierarchical structures can be further developed. Moreover, loading these sponges with different active materials also broadens the potential applications in various fields such as catalysis, sensors, electronics, energy devices, absorption, bioengineering, etc.^[33–38]

In summary, we develop a simple, completely controllable, binder and template free self-assembly methodology for the fabrication of macroscopic, ultralight (1–50 mg cm⁻³), and highly porous (97.5%–99.9%) 3D SACNT sponges. These SACNT sponges are in a honeycomb-like hierarchical 3D structure, combining micro-, meso-, and macropores together. In these sponges, SACNTs are connected into a continuous network through the strong van der Waals force, without using any

organic binder as most ordinary CNT sponges or aerogels often do. Therefore, the intrinsic excellent conductive properties and thermal/chemical stability of SACNTs can be preserved. Using SACNT sponges as templates, various materials (metals, metal oxides, composites) with adjustable honeycomb-like structure can be obtained, demonstrating great potential in massive manufacture and broad fields of applications, such as electronics, energy storage, bioengineering, catalysis, etc.

Experimental Section

Materials: SACNT arrays (diameter: 10–20 nm, height: 300 or 10–20 μm) were synthesized on silicon wafers in a low pressure chemical vapor deposition (LP-CVD) system. Details of the synthesis procedure can be found in previous works.^[39,40] Fabrication of SACNT arrays has already been successfully scaled up to meet the industrial requirements. Other CNTs include CNT-1 (arrays, 10 nm in diameter and 10 μm in height, Tiannai Ltd., China), CNT-2 (powders, 20 nm in diameter and 10 μm in length, Chengdu Organic Chemicals Ltd., China), and CNT-3 (powders, 10 nm in diameter and 10 μm in length, Tiannai Ltd., China).

Fabrication of SACNT Sponges by a Self-Assembly Method: Typically, 50 mg SACNTs were added into 50 mL deionized water in a 100 mL beaker, and dispersed for 45 min using an intensive ultrasonication probe (power: 350–450 W). The mixture was then poured into a desired mold and underwent freeze-drying for about 24 h. The product was a freestanding 3D sponge with density of 1 mg cm^{-3} and volume of about 50 cm^3 . By changing the concentrations of the suspensions, pure SACNT sponges with densities of 1–50 mg cm^{-3} can be achieved. The porosities of the SACNT sponges were calculated based on their apparent densities and the density of SACNT at 2 g cm^{-3} .

Fabrication of CNT Sponges with SDS: CNTs were dispersed in water with SDS as surfactant using an intensive ultrasonication probe (power: 300 W) for 30 min. In this suspension, the weight fraction of CNT was controlled at 10 mg mL^{-1} , and the weight ratio of CNT:SDS was 1:5. The suspension was standing for 24 h, and then underwent freeze-drying for 24 h.^[17] CNT–SDS sponges with density of 10 mg cm^{-3} were obtained.

Characterization: The electrical conductivities of the sponges were tested through a two-point method. The samples were all in the dimensions of 1 $\text{cm} \times 1 \text{cm} \times 1 \text{cm}$, and connected to a Keithley 2400 Source Meter. A linear voltage sweep from –1 to 1 V was loaded on the sponges, and the currents flowing through the sponges were recorded. The conductivity of the sponges can be calculated from the slope of the current–voltage sweep curves. TGA tests were conducted using a STA 449 C TGA (NETZSCH, Germany) at a heating rate of 10 $^\circ\text{C min}^{-1}$ between 25 $^\circ\text{C}$ and 1000 $^\circ\text{C}$ in air (or Ar). Compressive tests were performed using an Instron 5848 microtester at a strain rate of 10 mm min^{-1} and the dimensions of the samples were 1 $\text{cm} \times 1 \text{cm} \times 1 \text{cm}$. The electrochemical tests were conducted on a Land battery test system (Wuhan Land Electronic Co., China) based on coin-type (CR2016) half cells using TiO_2 @SACNT as the positive electrode and Li metal as the negative electrode.

Supporting Information

Supporting Information is available from the Wiley Online Library or from the author.

Acknowledgements

This work was supported by the National Basic Research Program of China (2012CB932301) and the NSFC (51102146 and 51472141).

- [1] C. T. White, T. N. Todorov, *Nature* **2001**, 411, 649.
- [2] S. Berber, Y. Kwon, D. Tománek, *Phys. Rev. Lett.* **2000**, 84, 4613.
- [3] L. Q. Liu, W. J. Ma, Z. Zhang, *Small* **2011**, 7, 1504.
- [4] K. L. Jiang, J. P. Wang, Q. Q. Li, L. A. Liu, C. H. Liu, S. S. Fan, *Adv. Mater.* **2011**, 23, 1154.
- [5] M. D. Lima, S. L. Fang, X. Lepro, C. Lewis, R. Ovalle-Robles, J. Carretero-Gonzalez, E. Castillo-Martinez, M. E. Kozlov, J. Y. Oh, N. Rawat, C. S. Haines, M. H. Haque, V. Aare, S. Stoughton, A. A. Zakhidov, R. H. Baughman, *Science* **2011**, 331, 51.
- [6] M. F. L. De Volder, S. H. Tawfik, R. H. Baughman, A. J. Hart, *Science* **2013**, 339, 535.
- [7] H. W. Zhu, B. Q. Wei, *J. Mater. Sci. Technol.* **2008**, 24, 447.
- [8] X. N. Zang, Q. Zhou, J. Y. Chang, Y. M. Liu, L. W. Lin, *Microelectron. Eng.* **2015**, 132, 192.
- [9] S. Park, M. Vosguerichian, Z. N. Bao, *Nanoscale* **2013**, 5, 1727.
- [10] Z. Y. Cao, B. Q. Wei, *Energy Environ. Sci.* **2013**, 6, 3183.
- [11] A. Lekawa-Raus, J. Patmore, L. Kurzepa, J. Bulmer, K. Koziol, *Adv. Funct. Mater.* **2014**, 24, 3661.
- [12] H. Choo, Y. Jung, Y. Jeong, H. C. Kim, B. Ku, *Carbon Lett.* **2012**, 13, 191.
- [13] L. Fan, C. Feng, W. M. Zhao, L. Qian, Y. Q. Wang, Y. D. Li, *Nano Lett.* **2012**, 12, 3668.
- [14] S. Nardecchia, D. Carriazo, M. L. Ferrer, M. C. Gutierrez, M. F. Del, *Chem. Soc. Rev.* **2013**, 42, 794.
- [15] X. C. Gui, J. Q. Wei, K. L. Wang, A. Y. Cao, H. W. Zhu, Y. Jia, Q. K. Shu, D. H. Wu, *Adv. Mater.* **2010**, 22, 617.
- [16] X. C. Gui, A. Y. Cao, J. Q. Wei, H. B. Li, Y. Jia, Z. Li, L. L. Fan, K. L. Wang, H. W. Zhu, D. H. Wu, *ACS Nano* **2010**, 4, 2320.
- [17] M. B. Bryning, D. E. Milkie, M. F. Islam, L. A. Hough, J. M. Kikkawa, A. G. Yodh, *Adv. Mater.* **2007**, 19, 661.
- [18] M. A. Worsley, S. O. Kucheyev, J. H. Satcher, A. V. Hamza, T. F. Baumann, *Appl. Phys. Lett.* **2009**, 94, 073115.
- [19] H. Y. Sun, Z. Xu, C. Gao, *Adv. Mater.* **2013**, 25, 2554.
- [20] S. Faraji, K. L. Stano, O. Yildiz, A. Li, Y. Zhu, P. D. Bradford, *Nanoscale* **2015**, 7, 17038.
- [21] B. You, J. H. Jiang, S. J. Fan, *ACS Appl. Mater. Interfaces* **2014**, 6, 15302.
- [22] M. A. Worsley, S. O. Kucheyev, J. H. Satcher, A. V. Hamza, T. F. Baumann, *Appl. Phys. Lett.* **2009**, 94, 73115.
- [23] G. N. Ostojic, *ChemPhysChem* **2012**, 13, 2102.
- [24] L. Lascialfari, C. Vinattieri, G. Ghini, L. Luconi, D. Berti, M. Mannini, C. Bianchini, A. Brandi, G. Giambastiani, S. Cicchi, *Soft Mater.* **2011**, 7, 10660.
- [25] X. T. Zhang, J. R. Liu, B. Xu, Y. F. Su, Y. J. Luo, *Carbon* **2011**, 49, 1884.
- [26] J. Chen, C. H. Xue, R. Ramasubramaniam, H. Y. Liu, *Carbon* **2006**, 44, 2142.
- [27] M. A. Worsley, P. J. Pauzauskie, S. O. Kucheyev, J. M. Zaugg, A. V. Hamza, J. H. Satcher, T. F. Baumann, *Acta Mater.* **2009**, 57, 5131.
- [28] K. L. Jiang, Q. Q. Li, S. S. Fan, *Nature* **2002**, 419, 801.
- [29] S. Luo, K. Wang, J. P. Wang, K. L. Jiang, Q. Q. Li, S. S. Fan, *Adv. Mater.* **2012**, 24, 2294.
- [30] Z. Y. Wu, C. Li, H. W. Liang, J. F. Chen, S. H. Yu, *Angew. Chem., Int. Ed.* **2013**, 52, 2925.
- [31] W. Q. Zhao, Y. B. Li, S. S. Wang, X. D. He, Y. Y. Shang, Q. Y. Peng, C. Wang, S. Y. Du, X. C. Gui, Y. B. Yang, Q. Yuan, E. Z. Shi, S. T. Wu, W. J. Xu, A. Y. Cao, *Carbon* **2014**, 76, 19.

- [32] W. Jiao, N. Li, L. Wang, L. Z. Wen, F. Li, G. Liu, H. M. Cheng, *Chem. Commun.* **2013**, 49, 3461.
- [33] Y. B. Yang, E. Z. Shi, P. X. Li, D. H. Wu, S. T. Wu, Y. Y. Shang, W. J. Xu, A. Cao, Q. Yuan, *Nanoscale* **2014**, 6, 3585.
- [34] M. Crespo, M. Gonzalez, A. L. Elias, L. P. Rajukumar, J. Baselga, M. Terrones, J. Pozuelo, *Phys. Status Solidi RRL* **2014**, 8, 698.
- [35] Y. Shen, D. Sun, L. Yu, Z. Wang, Y. Y. Shang, H. R. Tang, J. F. Wu, A. Y. Cao, Y. H. Huang, *Carbon* **2013**, 62, 288.
- [36] X. Xie, M. Ye, L. B. Hu, N. Liu, J. R. McDonough, W. Chen, H. N. Alshareef, C. S. Criddle, Y. Cui, *Energy Environ. Sci.* **2012**, 5, 5265.
- [37] H. B. Li, X. C. Gui, C. Y. Ji, P. X. Li, Z. Li, L. H. Zhang, E. Z. Shi, K. Zhu, J. Q. Wei, K. L. Wang, H. W. Zhu, D. H. Wu, A. Y. Cao, *Nano Res.* **2012**, 5, 265.
- [38] X. Y. Chen, H. L. Zhu, Y. C. Chen, Y. Y. Shang, A. Y. Cao, L. B. Hu, G. W. Rubloff, *ACS Nano* **2012**, 6, 7948.
- [39] X. B. Zhang, K. L. Jiang, C. Teng, P. Liu, L. Zhang, J. Kong, T. H. Zhang, Q. Q. Li, S. S. Fan, *Adv. Mater.* **2006**, 18, 1505.
- [40] K. Liu, Y. H. Sun, L. Chen, C. Feng, X. F. Feng, K. L. Jiang, Y. G. Zhao, S. S. Fan, *Nano Lett.* **2008**, 8, 700.